

Induced Active Sites by Adsorbate in Zeotype Materials

Guangchao Li^{1,2,3}, Christopher Foo^{2,5}, Xianfeng Yi¹, Wei Chen¹, Pu Zhao², Pan Gao⁴, Tatchamapan Yoskamtorn², Yao Xiao^{1,3}, Sarah Day⁵, Chiu C. Tang⁵, Guangjin Hou⁴, Anmin Zheng^{1*}, Shik Chi Edman Tsang^{2*}

¹State Key Laboratory of Magnetic Resonance and Atomic and Molecular Physics, National Center for Magnetic Resonance in Wuhan, Wuhan Institute of Physics and Mathematics, Innovation Academy for Precision Measurement Science and Technology, Chinese Academy of Sciences, Wuhan 430071, P.R. China

²Wolfson Catalysis Centre, Department of Chemistry, University of Oxford, Oxford OX1 3QR, U.K.

³University of Chinese Academy of Sciences, Beijing 100049, P.R. China

⁴State Key Laboratory of Catalysis, National Laboratory for Clean Energy, 2011-Collaborative Innovation Center of Chemistry for Energy Materials, Dalian Institute of Chemical Physics, Chinese Academy of Sciences, Dalian 116023, P.R. China

⁵Diamond Light Source Ltd., Harwell Science and Innovation Campus, Didcot, OX11 0DE, U.K.

*Correspondences' emails: edman.tsang@chem.ox.ac.uk (S. C. E. Tsang); zhenganm@wipm.ac.cn (A. M. Zheng)

Abstract

There has been a long debate on how and where active sites are created for molecular adsorption and catalysis in zeolites which underpin many important industrial applications. It is well accepted that Lewis acidic site (LAS) and basic site (LBS) as active sites in pristine zeolites are generally believed to be the extra-framework Al species and residue anion (OH^-) species formed at fixed crystallographic positions after their synthesis. However, the dynamic interactions of adsorbates/reactants with pristine zeotype materials to ‘create’ sites during the real condition remains largely unexplored. Herein, direct experimental observation of establishment of induced active sites in silicoaluminophosphate (SAPO) by adsorbate is *for the first time* made, which contradicts the traditional view of the fixed active sites in zeotype materials. Evidence shows that induced Frustrated Lewis pair (FLP, three-coordinated framework *Al* as LAS and SiO(H) as LBS) can be transiently favored for heterolytic molecular binding/reactions of competitive polar adsorbates due to their ineffective orbitals overlap in the rigid framework. High resolution magic-angle spinning solid-state nuclear magnetic resonance (MAS-SSNMR), synchrotron X-ray diffraction (SXR), neutron powder diffraction (NPD), in-situ Diffuse Reflectance Infrared Fourier Transform spectroscopy (*in-situ* DRIFT) and *ab initio* molecular dynamic (AIMD) demonstrate the transformation of a typical Brønsted acid site (BAS, Al(OH)Si) in SAPOs zeolites to new induced FLP structure for heterolytic binding upon adsorption of strong polar adsorbate. Our unprecedented finding opens up a new avenue to understanding of the dynamic establishment of active sites for adsorption or chemical reactions under molecular bombardments to zeolitic structures.

Introduction

Zeolites are the well-known solid catalysts, taking advantage of their unique molecular sieving effect, excellent catalytic activity and high thermal stability, they have been widely applied as heterogeneous catalysts in the large-scale industrial processes.¹ Even though they have enjoyed significant commercial success, many mechanistic aspects of fundamental information of zeolites are still under debate like the local structure of the active sites from the atomic level. The classical view of active sites for molecular adsorption or reaction such as Brønsted acid site (BAS) and Lewis acid site (LAS) in the Al-Si zeolites are generally believed to be on a proton attached oxygen bridge between substituted Al and Si ($\text{Si-O}^-(\text{H}^+)-\text{Al}$) due to charge balance and extra-framework Al species, respectively formed at fixed crystallographic positions on the zeolite structures after their synthesis. In fact, the Si-OH-Al bridge which can be displayed as $\text{Si-O}^-(\text{H}^+)-\text{Al}$, emphasizing the classical ion-exchange role of the proton, could also be described as $\text{SiO}(\text{H}) \rightarrow \text{Al}$, i.e., the dative coordinative bond between a lone electron pair of SiO(H) oxygen (electron rich) to a three-fold coordinated Al atom (electron deficient),² where the resonance form³ of Brønsted and Lewis acid sites in zeolites that may thus be interconverted dependent on environment. Dehydroxylation of zeolite Brønsted sites at high temperature appears to support the formation of Lewis acid sites in three-fold coordination.⁴ In addition, there are some recent intriguing observations to indicate that the framework of zeolites may not be regarded as a static structure.⁵ Treacy et al.⁶ argued that most of the existing zeolite frameworks are flexible when modeled as pure silica polymorphs. The flexibility of the zeolites structures has been implied by both theoretical calculations and catalytic experiments.^{5, 7} By controlling the zeolites framework flexibility and pore topology, Corma et al.⁸ reported a new zeolites (ITQ-55) with high efficient separation of ethane and ethylene. Calero et al.⁹ also reported that the intrinsic structural flexibility would greatly affect the separation of similar compounds in STW-type zeolite.

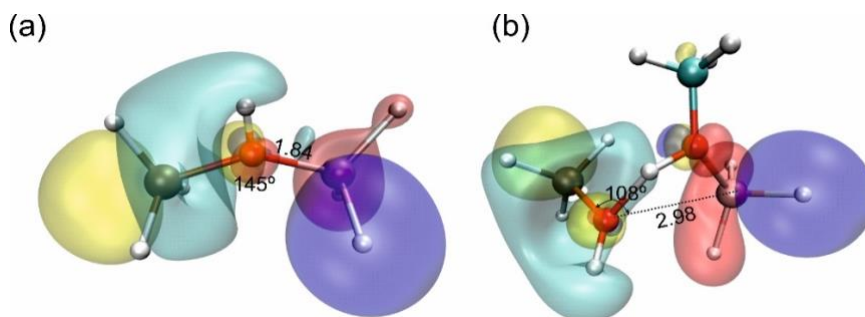
The SAPO class of zeolites has particularly attracted much attention due to its versatile catalytic properties in green chemistry, petrochemistry and refining.¹⁰⁻¹¹ Similar to normal alumino-silicate zeolites, the aluminophosphate molecular sieves consist of a tetrahedral oxide framework and the substitution of silica to them in the formation of the SAPO derivatives is described as a replacement of an (Al, P)-pair by two Si in the lattice. Altering the ratios among the Al, Si and P in different SAPO materials can generate BAS of variable quantities due to the charge compensation by protons as that of alumino-silicate zeolites. BAS over

these structures is attractive for fundamental mechanistic studies, as all the active sites in H-SAPO-34 may be considered equivalent in terms of their acid strength, steric accessibility, and transition state structures. However, with respect to the structure, there is a severe local distortion of the BAS T-O-T moiety from ideal tetrahedral symmetry due to the fact that the chemical nature of phosphorous is markedly dissimilar from Si and Al. Also, the local charge distribution can also play an important part in the structural distortion. Confirmed by both experiments and theoretical calculations, the distortion of bond lengths and angle of the BAS in SAPO results in a very different BAS to those in aluminosilicate zeolites.¹² Thus, the formation of Lewis acidic and basic sites from these structures during molecular adsorption/catalysis is anticipated to take place more readily than aluminosilicate zeolites. By combining in-situ synchrotron-radiation X-ray powder diffraction and DFT calculations, Arstad et al.⁷ demonstrated that the structure of SAPO-37 can collapse after adsorbing water molecules under 345 K. A similar observation was reported by Sliverwood et al.¹³ who showed that the SAPO-34 framework contracts following ammonia adsorption by using a neutron scattering technique. Using SSNMR and DFT calculations, Morris and Ashbrook et al.¹⁴⁻¹⁵ confirmed that framework Al-O bonds in zeolites can be reversibly broken through the adsorption and desorption of water at room temperature. Very recently, Liu et al.¹⁶ observed the same phenomenon using SSNMR. All of these observations indicate that the BAS structure is not completely stable and possesses some unquenched reactivity. However, despite these reports, it is not yet clear how and why such structural distortions occur.

On the other hand, it is recently established a frustrated Lewis pair (FLP) in homogeneous systems. This is a chemical entity containing both a Lewis acid (LA) and a Lewis base (LB) with unquenched activity at sterically hindered or rigid positions, which accordingly cannot undergo acid-base dative adduct formation. The FLP chemistry tends to take place in polar media with ionic species for the charge (electron pair) redistribution. Since the landmark report from Stephan et al.,¹⁷ the chemistry of FLP has been successfully developed during the last decades in several multiple research systems to activate and catalyze a wide range of substrate molecules. The concept of FLP has also been extended from the homogeneous area to heterogeneous system¹⁸. A large number of corresponding works have been reported, including dimensional materials,¹⁹ MOFs,²⁰⁻²¹ Au-Pt/Wox,²² Pt_x-loaded zeolite NaY,²³ B(C₆F₅)₃-molecular sieves,²⁴ polymers,²⁵ CeO₂,²⁶⁻²⁷ In₂O₃,²⁸⁻²⁹ and so on. Many new reactions have been found, and a great variety of different FLPs have been devised, characterized, and related reactions reported.¹⁷

In this work, using state-of-the-art techniques such as MAS-SSNMR, SXRD, NPD, in-situ DRIFT and DFT, we report *for the first time* that Lewis acid and basic sites in SAPO zeolites can be transiently created due to induced FLP via competitive adsorption of adsorbate molecules of increasing polarity such as acetone, ethanol, methanol, and water. Instead of establishing a rigid FLP in the previous reported homogeneous systems,³⁰ the traditional BAS in this class of SAPO zeolites represents a quenched but less stable dative adduct (Si-O(H)-Al) due to the strains and poor orbitals overlap imposed by the rigidity of the surrounding framework. We postulate that due to the instability, the adduct can be broken by the introduction of a stronger Lewis basic adsorbate molecule with polarity high enough to bind to framework Al as Lewis acid where silica hydroxyl as Lewis base hence new induced LA and LB sites to intercept with the adsorbate molecules. In this work, we adopted multi characterization techniques, in combination with molecular dynamics simulations, to provide a systematic and quantitative understanding of the new adsorbates induced active site in zeolites.

As shown in Scheme 1a, the BAS structure is maintained at a rigid static state. The HOMO is mainly located on the Al atom and the LUMO on the Si atom, with a T-O-T angle of 145° and Al-O distance of 1.84 Å. Upon adsorption of a polar molecule like methanol (Scheme 1b), it is shown that the HOMO expands to envelope the methoxy species which is indicative of a methoxy-to-Al charge transfer, forming a fully quenched Al-O-CH₃ moiety. This also results in the effective cleavage of the framework Al-O bond, as observed by a highly extended inter-atomic distance (2.98 Å) and a relaxed T-O-T angle (108°). Thus, the traditional BAS was induced to form FLP sites by heterolytic binding of methanol at the more stable coordinated state.



Scheme 1. **An illustration for induced FLP sites for competitive binding of methanol.** HOMO and LUMO of zeolite clusters extracted from optimized periodic H-SAPO-34 zeolite with replacing terminal Al and Si by H before (a) and after adsorption of methanol (b), purple (+ve) and red (-ve) for HOMO, cyan (+ve) and yellow (-ve) for LUMO. For models, H: white, O: red, Al: pink, C: cyan, Si: sepia. The optimized bond distances and angles with and without methanol generally match with diffraction data. It is shown that a significant stabilization

for HOMO around the Al by the charge transfer of methoxy converting the A-O(H)-Si BAS to induced FLP sites for heterolytic binding of methanol with subtle changes in bond lengths and angles (refer to Fig. S18).

Results and discussion

Acetone adsorption on SAPO zeolites. The supply of zeolite samples, pretreatments, the basic characteristics of the zeotype materials and zeolites including Transmission electron microscope (TEM) (Fig. S1), Laboratory X-ray diffraction (XRD) (Fig. S2a), N₂ adsorption isotherms (BET) (Fig. S2b, Table S1)) studies are summarized in **Supporting Information (SI)**. SSNMR is a conventional yet powerful classical tool to study Brønsted and Lewis acid sites in catalytic materials, as it provides a unique insight into structural and dynamic properties of solids at the atomic level.³¹⁻³² Both quantitative and qualitative information with high resolution and sensitivity can also be achieved. Before the adsorption experiment using ¹³C-2-acetone, ¹H, ²⁷Al, ²⁹Si, ³¹P SSNMR (detailed parameters of SSNMR experiments are given in **SI**) characterizations were performed (Figs. S3-9) which show the presence of typical BAS in the pristine samples with values agreeable to literature.^{31, 33-34} Curve in Fig. 1a shows the ¹³C cross-polarization (CP) magic-angle spinning (MAS) NMR spectra of H-SAPO-34 zeolite adsorbed with ¹³C-2-acetone. Interestingly, two peaks at 217 ppm (type-I) and 225 ppm (type-II) are clearly observed. According to the previous literature,³⁵ the major peak at 217 ppm is attributed to ¹³C-2-acetone adsorbed on BAS. However, the other ¹³C resonance at 225 ppm persistently appears in repeated measurements but remained ambiguous. One may consider the signal at 225 ppm to be attributed to the acetone adsorbed on the stronger BAS,³⁵⁻³⁶ and/or acetone adsorbed at surface defects.³⁴ In contrast, ¹H, ²⁷Al, ²⁹Si, ³¹P MAS SSNMR (Figs. S3-6) and ¹H-¹H DQ-SQ MAS NMR (Fig. S7) spectrum of H-SAPO-34 show that only BAS is present (when dried), while no framework defects are observed. Furthermore, when the samples were exposed to humidity at 298 K as shown in Fig. S10, the peak intensity of the 225 ppm vanished rapidly over increasing exposure time. A similar trend was also observed in the ³¹P signal of trimethylphosphine oxide (TMPO) pre-adsorbed on zeolites, indicating the presence of Lewis acid sites that vanish on exposure to moisture-containing air.³⁷ Therefore, we assigned the minor 225 ppm peak to ¹³C-2-acetone adsorbed at LAS. The analysis of 2D ¹³C-¹H hetero-nuclear correlation (HETCOR) NMR spectra further supports our assignment as shown in Fig. 1d. A dominant correlation peak at (217, 12) ppm corresponding to the ¹³C-2-acetone adsorbed on the BAS is anticipated; however, no correlation signal is observed between the 225 ppm and the proton of BAS ($\delta_H > 10$ ppm), with the exception

of the signal at (225, 7-10) ppm. Since ^1H chemical shift inside zeolites at 7-10 ppm can be assigned to the hydrogen-bonded silicon hydroxyl group,³⁸ we assigned this signal at (225, 7-10) ppm to ^{13}C -2-acetone adsorbed at LAS that are in close proximity to a hydroxyl group. The spatial relationship of 217 ppm and 225 ppm peaks was studied by 2D ^{13}C - ^{13}C PDSD NMR (Fig. 1e) which shows that there is a strong cross-peak pair at (217, 225) ppm and (225, 217) ppm, indicating that the carbon atoms associated with the signals at 225 and 217 ppm are in close proximity. Thus, we have shown using SSNMR that acetone not only adsorbs primarily at BAS but the LAS as well, and that the two adsorption species are in close proximity. The dependence of the LAS on the presence of acetone is the key question to resolve.

In order to directly visualize the configurations of adsorbates in zeolites, the combination of high-resolution synchrotron X-ray powder diffraction (SXRD) and neutron powder diffraction (NPD) were adopted. It is well known that both SXRD and NPD are powerful techniques in the high resolution determination of the crystallographic positions of adsorbates, such as ammonia, methanol, carbon dioxide and ethane, in porous crystalline materials including zeolites and metal-organic frameworks.³⁹⁻⁴² Crystal structures have been refined against the diffraction data using the whole-pattern Rietveld method, yielding the spatial relationships between guest species and host frameworks. In particular, bond distances and angles at the adsorption sites were measured with acceptable experimental errors, which offers complementary information to the SSNMR analysis.

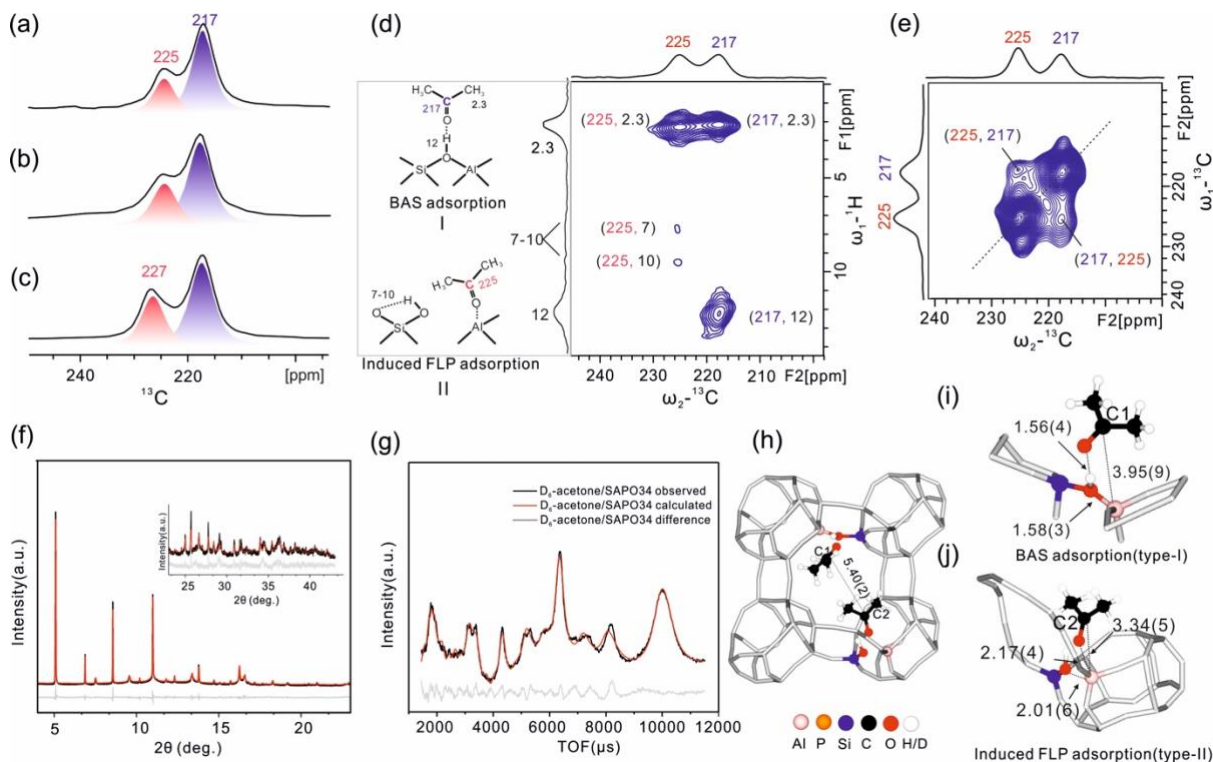


Fig. 1. Adsorption structures of acetone over H-SAPO-34. ^{13}C Cross-Polarization MAS NMR spectrum of ^{13}C -2-acetone adsorbed on H-SAPO-34 (a), H-SAPO-18 (b), H-SAPO-35 (c), 2D ^{13}C - ^1H HETCOR MAS NMR spectra with a contact time of 4 ms in right of (d), Schematic depicts the proposed the signals assignment of acetone BAS and induced FLP adsorptions in left of (d) and ^{13}C - ^{13}C PDS MAS NMR spectra of ^{13}C -2-acetone adsorbed on SAPO-34 zeolite(e), all the data were collected on Bruker Avance III 400 WB spectrometer using 4mm rotor at a spinning speed of 10 kHz at 298K. Data analysis was performed on Bruker TopSpin. SXR data measured at 298 K of acetone in H-SAPO-34 ($R_{\text{wp}} = 8.9\%$, $\chi^2 = 1.97$) (f), NPD data measured at 298K of D_6 -acetone in H-SAPO-34 ($R_{\text{wp}} = 1.9\%$, $\chi^2 = 2.27$) fitted by Rietveld refinement in TOPAS Academic 6 (g), SXR data in the range of 25-45° are expanded to illustrate the quality of Rietveld refinement. Due to the low scattering of light elements such as H by SXR, NPD was adopted to determine the H/D location. Crystallographic model based on both SXR and NPD Rietveld refinement (see Fig. S14 for further details) (h), acetone adsorbed on BAS, type-I(i) and the framework Al site, type-II (symmetry in adsorption sites is disregarded for clarity (j). the atomic and crystallographic parameters are summarized in Tables S5, 7, 8, 10).

The refined structure of deuterated acetone/H-SAPO-34 is depicted in Figs. 1f-j and S14: two adsorption states are also observed that are attributed to two types of adsorption sites (type-I: acetone on a BAS and type-II acetone on framework Al). These coexist inside the cage with the interatomic distance between C1 in type-I acetone and C2 in type-II acetone of 5.40(2)Å (Fig.1h), which falls within the detectable range of the 2D ^{13}C - ^{13}C PDS NMR. The occupancies and atomic positions of the two species in type-I and type-II are presented in Tables S7 and S10 which match well with the NMR estimation of their amounts as 3:1. Thus, the positions and occupancies of the two adsorbed acetone states have been quantitatively defined within the unit cell and in relation to each other by both SSNMR and crystallographic methods, which are in good

agreement. For the acetone type-I state, the inter-atomic angles and bond distances of Si-O(H)-Al (Al1-O3(H)-Si1:146.8°; T-O: 1.6-1.9 Å⁴³) are characteristic of BAS in H-SAPO-34, and the distance of the acetone C=O from H (BAS) of ca. 1.58(3) Å (Fig. 1i) is indicative of typical hydrogen bonding⁴⁴. On the other hand, for acetone type-II state, the adsorption geometry of C=O is clearly leaning toward the framework Al (LAS) (Fig. 1j), exhibiting an inter-atomic distance much shorter than in acetone type-I state (2.17(4) Å vs. 3.25(7) Å). Additionally, the [Al-O-Si] bond angle of 146.8° found in typical BAS is significantly lowered to 124.3° [Al5-O4-Si2] and the Al-O bond distance is increased to 2.01(6) Å indicating the weakening of the Al-O interaction in the acetone type-II mode (Fig. S14). These changes in geometry are attributed to some conversion of adsorption of acetone from type-I to type-II via the induced reconstruction (Fig. S14). Further structural information on the unusual acetone type-II state at LAS was observed in the dipolar interaction between the ¹³C atom of acetone with framework ²⁷Al atoms by using ¹³C-²⁷Al symmetry-based rotational-echo saturation-pulse double-resonance (SRESPDOR), which is based on the inter-nuclear dipolar interaction/distance (Fig. S11). Signals of 217 ppm (type-I) and 225 ppm (type-II) are both subject to a ¹³C-²⁷Al dipolar dephasing, which clearly shows that the ¹³C-2-acetone of 225 ppm is indeed in a very close proximity to the aluminum species. Due to the close proximity of acetone and the Al atoms in the framework, the resonance peak at 225 ppm is subject to a more intense dipolar dephasing than that of 217 ppm. These crystallographic values match with the expectation of the induced formation of LAS for binding of electron-donating C=O of acetone as shown in our refined crystal structure (Figs. 1i-j and Fig. S14). Based on the afore-mentioned experimental evidence, new insights into the absorption states of ¹³C-2-acetone over H-SAPO-34 zeolite are thus obtained (Fig. 1d left). As well as the anticipated adsorption at the typical BAS in H-SAPO-34 in which acetone adsorbs at the bridging-hydroxyl proton (217 ppm), some acetone has been shown to coordinate directly with framework Al atoms (225 ppm).

In order to investigate the origin and driving-force behind the unusual acetone type-II state, other SAPO zeolites (H-SAPO-18 and H-SAPO-35) were studied using similar methods. Basic structural information based on 1D ¹H, ²⁷Al, ²⁹Si, ³¹P MAS SSNMR and 2D ¹H-¹H DQ-SQ MAS SSNMR spectra are provided as shown in Figs. S3-9, except a small amount of silanol groups inside H-SAPO-18 zeolite (Figs. S3c and S9), no obvious extraframework Al species are detected in H-SAPO-18 and H-SAPO-35. The detailed peaks assignments which are matching well with the literature results are discussed in the supporting information

(Table S11). Upon adsorption of ^{13}C -2-acetone, similar results were also observed in the ^{13}C chemical shifts of these samples, as shown in Figs. 1b-c. For both samples, two ^{13}C signals were also observed (H-SAPO-18: 217 ppm and 225 ppm; H-SAPO-35: 217 ppm and 227 ppm). Peaks at 225 ppm in H-SAPO-18 and 227 ppm in H-SAPO-35 vanished after adsorption of water (Figs. S12a and S12c), which can be assigned to acetone adsorbed on framework Al atoms (induced FLP). 2D ^{13}C - ^1H HETCOR MAS NMR spectrum also support our assignment showing the correlation between carbonyl carbon and proton in BAS, i.e. (217, 12.2) ppm in H-SAPO-18 (Fig. S12b) and (217, 12.7) ppm in H-SAPO-35 (Figs. S12d). Also, according to the 2D ^{13}C - ^{13}C PDSD NMR spectrum, these two ^{13}C -2-acetone species in both H-SAPO-18 and H-SAPO-35 are also close to each other (Figs. S12e-f).

Accordingly, there are two types of FLP reported in literature (Fig. S13):^{18, 45} one is the intermolecular FLP and the other one is intramolecular FLP. Stephan et al.⁴⁶ recently reported an intramolecular phosphane–borane adduct that can be opened up to activate dihydrogen dissociatively. With reference to the type-II state of acetone, Brønsted acid site in SAPOs appears to act as an intramolecular FLP like structure. For Al-O(H)-Si moiety, Al and Si-O are initially confined by the surrounding rigid zeolites framework, however Al-O dative bonds can be cleaved to a degree to form induced intramolecular FLP after the adsorption of acetone by C=O binding to the Al atom. Given that FLPs are well-known to activate small molecules, including H_2 , CO_2 , SO_2 , NO , CO , N_2O , olefins, methanol,⁴⁷ methanol adsorption was further conducted by the SAPO zeolites.

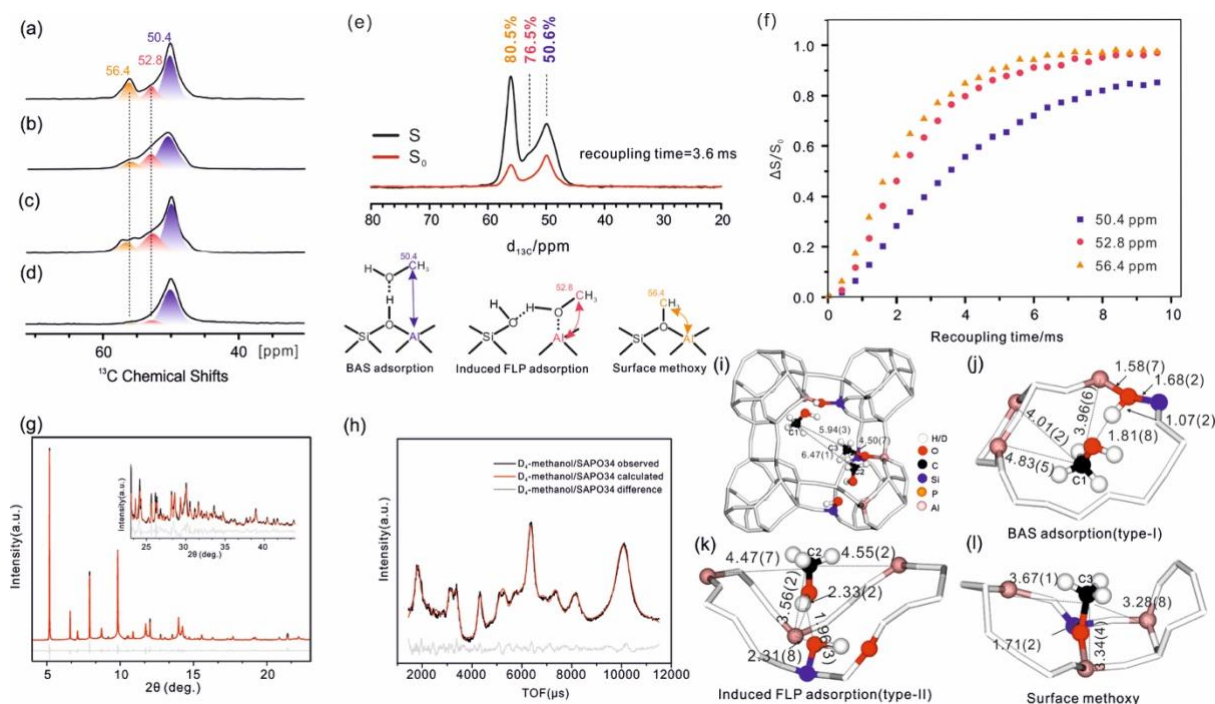


Fig. 2. Adsorption structures of methanol over H-SAPO-34. ^{13}C Cross-Polarization MAS NMR spectrum of ^{13}C -methanol adsorbed on H-SAPO-34(a), H-SAPO-18(b), H-SAPO-35(c), H-SSZ-13(d), ^{13}C - ^{27}Al -S-RESPDOR spectra of ^{13}C -methanol adsorbed on H-SAPO-34 in top of (e), Schematic depicts the proposed the signals assignment of BAS adsorption, FLP adsorption and the surface methoxy species in bottom of (e), ^{13}C - ^{27}Al -S-RESPDOR built-up data of signals at 50.4 ppm (purple square), 52.8 ppm (red dots) and 56.4 ppm (yellow triangle) (f), all the data were collected on Bruker Avance III 400 WB spectrometer using 4mm rotor at a spinning speed of 10 kHz at 298K. Data analysis was performed on Bruker TopSpin. SXR data measured at 298K of methanol in H-SAPO-34 ($R_{\text{wp}} = 9.4\%$, $\chi^2 = 10.34$) (g), NPD data measured at 298K of D_4 -methanol in H-SAPO-34 ($R_{\text{wp}} = 1.4\%$, $\chi^2 = 1.6$) fitted by Rietveld refinement in TOPAS Academic 6 (h). SXR data in the range of 25 – 45° are zoomed to illustrate the quality of Rietveld refinement. Due to the invisibility of light elements like H by SXR, NPD was adopted to detect the H/D location. Crystallographic model based on both SXR and NPD Rietveld refinement (i), methanol adsorbed on BAS, type I (j) and the framework Al site, type II (k), and the formed surface methoxy species (see Fig. S18 for further detail) (l). Symmetry in adsorption sites is disregarded for clarity. The atomic and crystallographic parameters are summarized in Tables S5, 6, 7, 9.

Methanol adsorption on SAPO zeolites. Figs. 2a–c show the ^{13}C CP MAS SSNMR spectrum of ^{13}C -methanol adsorbed on H-SAPO-34, H-SAPO-18, and H-SAPO-35 zeolites, respectively at 298K. In contrast to acetone adsorption, in which two signals that correspond to the two adsorption modes are deconvoluted, for methanol the Gaussian deconvolution clearly show three peaks at 50.4 ppm, 52.8 ppm and 56.4 ppm, respectively. The lowest chemical shift signal at 50.4 ppm can easily be assigned to methanol adsorbed at BAS (C1 in type-I), as it perfectly matches the literature value.⁴⁸ A small signal at 52.8 ppm, which is clearly observable on all the zeolites but almost negligible in H-SSZ-13 (Fig. 2d). This can be attributed to methanol coordinated to the framework Al of BAS to form the induced FLP state (C2 in type-II), which matches to the chemical shift of $\text{CH}_3\text{O}-\text{Al}$ species.⁴⁹ Interestingly, the 56.4 ppm peak, which corresponds to the typical NMR chemical shift of surface methoxy species (C3 of SMS),⁴⁸ is unexpectedly obtained at room

temperature. However, this may be accounted for by considering that polar methanol is vulnerable to dehydration, especially from the induced FLP state at mild conditions.

Methanol adsorption over H-SSZ-13 zeolite which processes the same structure with that of H-SAPO-34 but with a different framework composition (Si, Al, for H-SSZ-13, P, Al for H-SAPO-34) was also studied in order to investigate the role of phosphorous in the system (^1H , ^{27}Al MAS SSNMR spectrum of pristine H-SSZ-13 and its ^{13}C MAS SSNMR result after ^{13}C -2-acetone adsorption are displayed in Fig.S24). As shown in Fig. 2d, it exhibits very dominant adsorption as type-I, and a very low proportion of adsorbed methanol in the type-II or as SMS (52.8 and 56.4 ppm). It is noted that the typical distance of Al-O over pristine H-SSZ-13 is markedly shorter than those of the other pristine SAPO samples.¹² The shorter bond and more efficient orbital overlap forms a more stable LA-LB adduct in Al-O-Si, which is less prone to cleavage and the formation of the induced FLP and then to SMS. Thus, we show that the presence of phosphorous increases the proportion of adsorbed methanol bound both to the induced FLP and as SMS. Quite logically, it is suggested that the longer Al-O bond and unbalanced charge after phosphorus introduction are more likely to make it cleaved by the adsorption of small polar molecules, leading to the type-II state that we have comprehensively characterized by complementary crystallographic and NMR methods.

The ^{13}C - ^{27}Al S-RESPDOR was then performed to qualitatively compare the distance between the methanol carbon and Al in the zeolite framework. When the recoupling time was set at 3.6 ms (top of Fig. 2e), the strongest dipolar ^{13}C - ^{27}Al dephasing attenuation (80.5%) is observed on the 56.4 ppm peak, followed by the 52.8 ppm peak (76.5%) and then the 50.4 ppm peak (50.6%). From the simulated dephasing curve (Fig. 2f), the degrees of attenuation, which is inversely proportional to the ^{13}C - ^{27}Al distance, generally match well with the experimental measurements collected at 3.6 ms (top of Fig. 2e). Notice that there is more than one Al atom interacting with the C-Al in proximity in the SAPO zeolites. This effect on the diphasic ^{13}C - ^{27}Al S-RESPDOR interaction makes it very difficult to derive the actual distances between the methanol carbon and Al. However, the order reflects inversely to the distance between the ^{13}C and ^{27}Al corresponding to SMS (56.4 ppm), induced FLP adsorption (52.8 ppm) and BAS adsorption (50.4 ppm), respectively (Fig. 2f).

For their refined crystal structures from SXRD/NPD with deuterium methanol, the geometric adsorption modes of methanol on SMS, induced FLP and BAS of H-SAPO-34 for the three types can be obtained (Figs.

2g-l and Fig. S18). For the type-I methanol adsorption mode, it seems to be a typical BAS adsorption over the pristine H-SAPO-34, with an Al-O-Si angle of 145.9° (Al4-O5-Si3) and typical inter-atomic distances (Fig. 2j and Fig. S18). It is striking that in the methanol type-II adsorption geometry here (C2-methanol on Al5 in Fig. 2k and Fig. S18), the elongated Al-O bond length (2.31(8) Å) and compressed Al-O-Si angle (118.4°) are very similar to the type-II state of acetone on induced FLP as previously shown by SXRD/NPD, which appears to be greatly stretched from the typical value of 1.58(7) Å in the acetone type-I state (Fig. 1j).¹² Notably, a hydrogen-bond between the H of methanol and the O of silanol is observed by NPD ($\text{H}\cdots\text{O}$ distance at 1.96(3) Å). From the refined model (Fig. 2l and Fig. S18), it is observed that SMS species (C3-methanol on Al4) after methanol dehydration is attached to Al with the shortest distance of 3.34(4) Å, which is in agreement with the analysis of the strongest interaction of ^{13}C - ^{27}Al S-RESPDOR data (Fig. 2f). Fig. 2e (bottom) summarizes the schematic adsorption structures according to the three refinement structures.

Their corresponding spatial distances of methanol adsorption modes in type-I (C1), type-II (C2) and SMS (C3) to each other in a unit cell of the refined crystal can be directly measured as ca. 4.50(7) Å for C2-C3, 5.94(3) Å for C1-C3 and 6.47(1) Å for C1-C2, respectively (Figs. 2i and S18). These species in such short distances could be reflected from 2D NMR. Indeed, 2D ^{13}C - ^{13}C PDSD NMR gave the correlation peaks of dominant C1 and C3 species at (50.4, 56.4) ppm and (56.4, 50.4) ppm (Fig. S15 for H-SAPO-34, Fig. S16 for H-SAPO-35, Fig. S17 for H-SAPO-18) indicative of their spatially close proximity (the interaction of C1 with the smallest C2 species cannot be resolved well). According to their occupancy values (Table S9), the C atom ratio of methanol-BAS (type I) to the summed methanol-LA and SMS (produced from induced FLP) in unit cell of the crystal corresponds to ca. 1.3 ± 0.3 , which is also in good agreement with the value obtained from the NMR data (Table S4).

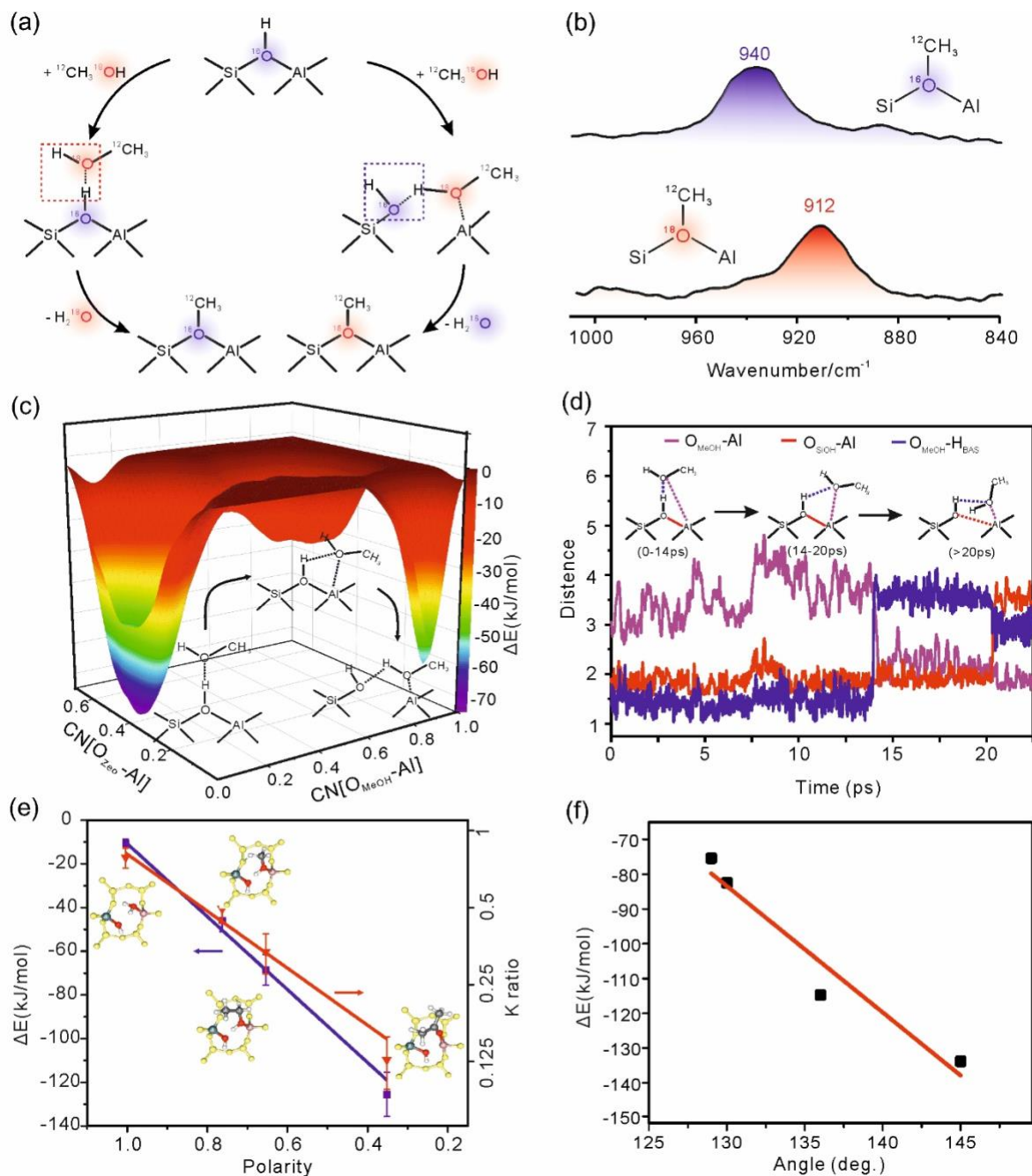


Fig. 3. In situ DRIFT and DFT Calculations. Schematic depicts the mechanisms of the formation of surface methoxy species via the traditional BAS route and our proposed induced FLP route (a), in-situ DRIFT experiments showing the C-O stretching vibration peak position of methoxy species for samples of ¹⁶O-methanol/H-SAPO-34 (purple) and ¹⁸O-methanol/H-SAPO-34 (red) (the data were collected on Nicolet iS50 FT-IR spectrometer with a high temperature, high pressure DRIFT reaction cell using an MCT/A detector, 64 scans and at a resolution of 4 cm⁻¹) (b), 3D diagram of the coordinating number changes for methanol adsorbed on H-SAPO-34 with the transformation from BAS adsorption state to induced FLP adsorption state during the AIMD simulations x-axis: coordinating number of O_{MeOH}-Al (CN[O_{MeOH}-Al]); y-axis: coordinating number of O_{Zeo}-Al (CN[O_{Zeo}-Al]), z-axis: free energy change of various states from high to low in kJ/mol (red to purple) (c), the changes of bond distance for methanol adsorbed on H-SAPO-34 with the transformation from initial BAS adsorption state to induced FLP adsorption state during the AIMD simulations Purple: distance between O of methanol and framework Al (O_{MeOH}-Al), Red: distance between O and Al of BAS (O-SiOH-Al), blue: distance between O of methanol and H of BAS (O_{MeOH}-H_{BAS}) (d), the free energy change (adsorption state - ground state, purple line) and K ratio (type-II+ surface-alkoxy)/(all

adsorption states) – red line) of H-SAPO-34 as the function of polarity of various adsorbates (acetone, ethanol, methanol, water) (e), the relationship between free energy change and hypothetical angles of BAS (Al-O(H)-Si) of H-SAPO-34 zeolite (f).

There have been various discussions on the mechanism of methanol to olefin (MTO) reaction in zeolite topologies including CHA,⁵⁰ MFI,⁵¹ Beta.⁵² For the formation of SMS, it is traditionally accepted that methanol is adsorbed on BAS by a strong hydrogen-bonding interaction between the bridging-hydroxyl proton of BAS and the oxygen of methanol,⁵³ followed by dehydration and the loss of water (Fig. 3a left and S19). However, on normal alumino-silicate zeolites this reaction usually only occurs at high temperature (> 400 K, Fig. S19).⁵⁴ Surprisingly, we clearly observe a small amount of methanol dehydration to SMS take place at room temperature over SAPO zeolites (Figs. 2a-c). This suggests a fundamentally different reaction pathway for this process. For SMS, it is postulated that the methoxy species is initially directly bonded to the framework Al in the induced FLP state (Fig. 3a right) with its hydroxyl proton is attached to the Lewis base site (OH). This would then favor the heterolytic cleavage of the methanol. Subsequently, a water molecule is eliminated from -SiOH₂, reforming the conventional Lewis adduct Al-O-Si yielding the SMS. It is significant that there is no C-O cleavage in the methanol in this induced FLP route since the Lewis acidic Al is anticipated to strongly bond with the Lewis basic O. This is in contrast to the conventional BAS route which likely proceeds with C-O cleavage of methanol to eliminate H₂O. Crucially, in type-I dehydration, the resulting methoxy oxygen originates from the framework; meanwhile, in type-II dehydration, the resulting methoxy oxygen originates from the methanol.

In order to verify our conjecture, in-situ DRIFT experiments were performed at elevated temperature using ¹⁶O-methanol and ¹⁸O-enriched methanol separately.⁵⁵ When using non-labeled methanol the peak assigned to the stretching vibration of ¹²C-¹⁶O in methoxy species⁵⁶ appeared at 940 cm⁻¹ (Fig. 3b); meanwhile, for ¹⁸O-methanol the peak is clearly shifted to 912 cm⁻¹. This indicates that the methoxy oxygen in SMS is from the methanol, and hence formed by type-II methanol adsorption. In contrast, for the typical alumino-silicate zeolite H-SSZ-13 under identical conditions, there is no difference in the SMS stretching vibration when using unlabeled and ¹⁸O-methanol, which indicates that the SMS methoxy oxygen is from the framework, and is formed by type-I methanol adsorption (Fig. S20). Similar results are also observed in the common used H-ZSM-5 zeolites in which isotopic labeling has no effect on the peaks observed at 940 cm⁻¹ and 980

cm⁻¹ that were assigned to the C-¹⁶O stretching vibrations of SMS⁵⁷⁻⁵⁸ (Fig. S21). The results discussed above provide the possibility that induced FLP adsorption of methanol may be favorably formed in SAPO zeotype materials and zeolites for MTO reaction. However, other activation sites for the MTO reaction may have created at elevated temperature. Further experiment should also be performed under in situ or operando conditions. This preliminary work gives interesting implications on an alternative route for SMS species formation but it should be approached more carefully in further study.

Theoretical calculations. To further investigate the adsorption behavior of methanol on H-SAPO-34 zeolites, DFT calculations using VASP and ab initio molecular dynamic (AIMD) simulations were conducted (details of calculation methods and parameters are provided in **SI**). The coordinating number is a value proportionate to the bonding strength with 0 corresponds to no bonding and 1 to a chemical bond. 3D diagram of coordinating numbers and energy indicate that both the classical BAS adsorption state and the induced FLP adsorption state occur when methanol is introduced into the zeolite. In general, the larger the coordinating numbers, the stronger the corresponding. As shown in Fig. 3c, O_{Zeo}-Al (initial state) and O_{MeOH}-Al (final state) coordinating numbers are 0.85 and 0.45, respectively.

An initial state of type-I BAS-adsorbed methanol in H-SAPO-34 at 1 bar and 298K was modelled by AIMD and the reaction allowed to progress at the transient time. By analyzing several inter-atomic distances, it is observed that the type-I mode can be directly converted to the type-II induced FLP structure (Fig. 3d), i.e. methoxy directly bonded to the framework Al site (induced LA) and H to Si-OH site (induced LB) when temperature and pressure were taken into consideration to overcome the structural reorganization energy. Interestingly, it is shown that the conversion occurs in three distinct steps: 1) coordination of framework Al and methanolic oxygen to form a pseudo four-membered ring, 2) methanol moves close to the framework Al, and 3) cleaving of the framework Al-O bond. The process of the first step (0-14ps) to the second step (14-20ps) is observed in that the distance of the primary interaction in type-I adsorption between the bridging-hydroxyl proton and methanolic oxygen increases at 14 ps (O_{MeOH}-H_{BAS}: 1.7 Å to 3.5 Å), while simultaneously the distance between Al and methanolic oxygen decreases (O_{MeOH}-Al: 3.5 Å to 2.0 Å). After that, the third step occurs in the increase of the framework Al-O distance at 20 ps (O_{SiOH}-Al: 1.9 Å to 3.2 Å) and further decrease of the distance for O_{MeOH}-Al (2.0 Å to 1.9 Å) and O_{MeOH}-H_{BAS} (3.5 Å to 2.9 Å). Here it is shown by computational methods that conversion between the type-I and type-II adsorption mode is

possible, which occurs through a pseudo four-membered ring intermediate state. Similar results were also obtained based on acetone adsorption calculations (Figs. S22 and S23).

A further fundamental question to ask is how the nature of the adsorbate molecule affects type-II induced FLP adsorption and their related product. By using the increasingly polar adsorbates, acetone, ethanol, methanol and water as the NMR probe molecules, the K ratio of the normalized type II peaks (induced FLP + surface-alkoxy species) in reference to the total adsorbate by integrating their peak areas from the NMR data are given (Table S4, Figs. S25 and S26). Interestingly, we have discovered a linear relationship between the adsorbate polarity and their relative amount in the K ratio (Fig. 3e, red). The calculated FLP free energy changes are logarithmic correlated with the polarity, in which high polarity adsorbates give lower reorganization energy required to the induced FLP state from BAS state (Fig. 3e, purple). Undoubtedly, the thermodynamic preference for binding by cleaved Al as LA against O(H)Si in the induced FLP is highly dependent on the polarity of the molecule because greater availability of the adsorbate electron pair leads to greater Lewis basicity and reactivity with the LA Al site. The entropic contribution, solvency as well as charge stabilization in H-SAPO-34 are envisaged to overcome the lower reorganization energy and facilitate the FLP route from BAS. In summary, the more polar the adsorbate, the greater the proportion of adsorbate is bound in the type-II state and the stronger this binding is.

We have also excitingly found a correlation between the initial Al-O(H)-Si bond angle and the adsorption energy of methanol. The energies of various H-SAPO-34 clusters with fixed Al-O-Si bond angles between 120 and 150° were optimized using DFT calculations. We show that the greater the distortion from the typical zeolite angle of 145° results in linearly decreasing adsorption strength (Fig. 3f). The larger T-O-T angle gives higher adsorption energies. It means that BAS sites with the conventional zeolitic angle are easier to convert to induced FLP sites by competitive molecular adsorption and catalysis, relative to more distorted SAPO zeolites. We also anticipate that increasing temperature could increase the proportion of adsorption resulting in FLP geometry through type-I to type-II conversion, but further work is required to characterize the temperature dependence of these structures and overall system.

It is worth to note that functions of the zeolites as catalytic materials are strongly mediated by the detailed features of their acid sites.⁵⁹⁻⁶² The induced frustrated Lewis pairs formed by the adsorption of small polar molecule is beyond our conventional understanding of acid site in zeolites. The induced frustrated Lewis

pairs cannot be created by the classical ways. According to the previous literature, Lewis acid/basic sites in zeolites are generally considered to be created by the introduction of hetero-atoms during synthesis⁶³ or post treatment⁶⁴ and extra-framework Al (EFAL) species during de-alumination.⁶⁵ Various techniques including SSNMR,⁶⁶⁻⁶⁷ EXAFS,⁶⁸ TEM,⁶⁹ SXRD,⁷⁰ UV-vis⁷¹ as well as DFT calculations⁷² have been adopted to investigate their structures and properties. Poncelet et al.⁷³ reported three types of Al species in Beta which can be inter-transformed to each other. Koningsberger et al.⁷⁴ subsequently confirmed their presence by using in situ X-ray absorption near-edge spectroscopy. Dedecek et al.⁷⁵ demonstrated the formation of (SiO)₃Al from the de-hydroxylation of (SiO)₃AlOH in Ferrierte zeolite. These moieties are clearly in pre-existence for characterization but are very reactive and may be subject to site poisoning in handling. However, considering the fact that the generation and performance of active sites would be influenced by the beneath lattice atoms and the local environment, active sites in solid surface could also be generated in situ under reaction conditions.⁷⁶ Surface rearrangement/restructuring in contact with strong interacting adsorbate would occur under reaction condition that causes dynamic establishment of active sites.⁷⁷ In this work, we have demonstrated that induced intramolecular FLP sites are transiently created to bind with small polar molecules upon their adsorption/activation over H-SAPO zeolites, which contradicts the traditional view of acid sites structure in zeolites. Our finding provides a new understanding of acid site in SAPOs zeolites and we believe that the observation of this new binding mode can offer great insights into existing zeotype materials and zeolitic systems and exciting new prospects in transient catalysis in the future.

Conclusion

In summary, the combination of state-of-the-art solid-state NMR experiments, synchrotron X-ray powder diffraction, neutron powder diffraction, in-situ DRIFT and theoretical calculations has revealed the formation of transient active sites for adsorption/catalysis of small molecules. The classical view of rigid and stable zeolite materials with pre-existing active sites is not a complete description. Instead, we propose that zeolite structures could be labile, dynamic and fluxional due to ineffective orbitals overlap in distorted environments which make the structures responsive to environment. With regard to the catalytic implications, we demonstrate that the presence of induced FLP acid sites offers a new route to form the key surface-methoxy intermediate in methanol-to-olefin reactions over SAPO catalysts. This observation may provide implications on alternative route to be considered for in-situ generation of catalytic sites in the MTO process

and for other catalysis reactions under tailored reaction mixture.

Acknowledgments

The diffraction and refinement work and part of NMR studies were taken place at the University of Oxford, UK funded under the IUK- EPSRC grant (55872-383337) with the SXR D and NPD beamtimes (P2018121100019) allocated by Diamond Synchrotron Light Source, UK and China Spallation Neutron Source, respectively. Supports were also obtained by the National Natural Science Foundation of China (No. 22032005, 21802164, 21902180, 21991092, and 22002174). Natural Science Foundation of Hubei Province of China (2018CFA009), and Key Research Program of Frontier Sciences, CAS (QYZDB-SSW-SLH026). The authors thank Ping-Luen Ho and Kwan Chee Leung from Tsang group at Oxford for their assistance in further TEM and XRD characterization. GL gratefully thanks the financial support from China Scholarship Council (Grant No. 201804910472) to enable him to study at the University of Oxford. CF acknowledges the EPSRC-Diamond Light Source joint DPhil Scholarships, UK and for SXR D beamtimes for this work.

Supplementary materials

Experimental details, methods and additional results of XRD patterns, TEM images, N₂ adsorption isotherms, solid state NMR spectrum, structure refinements data including Figs. S1 to S26, Scheme S1-S3, Tables S1 to S12.

References

1. Kulprathipanja, S., *Zeolites in industrial separation and catalysis*. John Wiley & Sons: 2010.
2. Haag, W. O.; Lago, R. M.; Weisz, P. B., The active site of acidic aluminosilicate catalysts. *Nature* **1984**, *309* (5969), 589-591.
3. Barthomeuf, D.; Derouane, E. G.; Hölderich, W., *Guidelines for mastering the properties of molecular sieves: relationship between the physicochemical properties of zeolitic systems and their low dimensionality*. Springer Science & Business Media: 2013; Vol. 221.
4. Bolton, A.; Lanewala, M., A mechanism for the isomerization of the hexanes using zeolite catalysts. *Journal of Catalysis* **1970**, *18* (1), 1-11.
5. Sartbaeva, A.; Wells, S. A.; Treacy, M.; Thorpe, M., The flexibility window in zeolites. *Nature Materials* **2006**, *5* (12), 962-965.
6. Kapko, V.; Dawson, C.; Treacy, M.; Thorpe, M., Flexibility of ideal zeolite frameworks. *Physical Chemistry Chemical Physics* **2010**, *12* (30), 8531-8541.
7. Kalantzopoulos, G. N.; Lundvall, F.; Thorshaug, K.; Lind, A.; Vajeeston, P.; Dovgaliuk, I.; Arstad, B.; Wragg, D. S.; Fjellvåg, H., Factors Determining Microporous Material Stability in Water: The Curious Case of SAPO-37. *Chemistry of Materials* **2020**, *32* (4), 1495-1505.
8. Bereciartua, P. J.; Cantín, Á.; Corma, A.; Jordá, J. L.; Palomino, M.; Rey, F.; Valencia, S.; Corcoran, E. W.; Kortunov, P.; Ravikovitch, P. I.; Burton, A.; Yoon, C.; Wang, Y.; Paur, C.; Guzman, J.; Bishop, A. R.; Casty, G. L., Control of zeolite framework flexibility and pore topology for separation of ethane and ethylene. **2017**, *358* (6366), 1068-1071.

9. Bueno-Perez, R.; Balestra, S. R. G.; Cambor, M. A.; Min, J. G.; Hong, S. B.; Merkl, P. J.; Calero, S., Influence of Flexibility on the Separation of Chiral Isomers in STW-Type Zeolite. **2018**, 24 (16), 4121-4132.
10. Tian, P.; Wei, Y.; Ye, M.; Liu, Z., Methanol to Olefins (MTO): From Fundamentals to Commercialization. *ACS Catalysis* **2015**, 5 (3), 1922-1938.
11. Haw, J. F.; Song, W.; Marcus, D. M.; Nicholas, J. B., The Mechanism of Methanol to Hydrocarbon Catalysis. *Accounts of Chemical Research* **2003**, 36 (5), 317-326.
12. Sastre, G.; Lewis, D. W.; Catlow, C. R. A., Structure and stability of silica species in SAPO molecular sieves. *The Journal of Physical Chemistry* **1996**, 100 (16), 6722-6730.
13. Silverwood, I. P., SAPO-34 Framework Contraction on Adsorption of Ammonia: A Neutron Scattering Study. *Chemphyschem* **2019**, 20 (13), 1747-1751.
14. Heard, C. J.; Grajciar, L.; Rice, C. M.; Pugh, S. M.; Nachtigall, P.; Ashbrook, S. E.; Morris, R. E., Fast room temperature lability of aluminosilicate zeolites. *Nature communications* **2019**, 10 (1), 1-7.
15. Pugh, S. M.; Wright, P. A.; Law, D. J.; Thompson, N.; Ashbrook, S. E., Facile, Room-Temperature ¹⁷O Enrichment of Zeolite Frameworks Revealed by Solid-State NMR Spectroscopy. *Journal of the American Chemical Society* **2019**, 142 (2), 900-906.
16. Sun, T.; Xu, S.; Xiao, D.; Liu, Z.; Li, G.; Zheng, A.; Liu, W.; Xu, Z.; Cao, Y.; Guo, Q.; Wang, N.; Wei, Y.; Liu, Z., Water-Induced Structural Dynamic Process in Molecular Sieve under Mild Hydrothermal Conditions: A Novel Ship-in-Bottle Strategy for Acidity Identification and Catalyst Modification. *Angewandte Chemie-International Edition* **2020**, 59, 2-12.
17. Stephan, D. W., The broadening reach of frustrated Lewis pair chemistry. *Science* **2016**, 354 (6317), aaf7229.
18. Ma, Y.; Zhang, S.; Chang, C.-R.; Huang, Z.-Q.; Ho, J. C.; Qu, Y., Semi-solid and solid frustrated Lewis pair catalysts. *Chemical Society Reviews* **2018**, 47 (15), 5541-5553.
19. Primo, A.; Neatu, F.; Florea, M.; Parvulescu, V.; Garcia, H., Graphenes in the absence of metals as carbocatalysts for selective acetylene hydrogenation and alkene hydrogenation. *Nature Communications* **2014**, 5 (1), 5291.
20. Ye, J.; Johnson, J. K., Design of Lewis Pair-Functionalized Metal Organic Frameworks for CO₂ Hydrogenation. *ACS Catalysis* **2015**, 5 (5), 2921-2928.
21. Ye, J.; Johnson, J. K., Screening Lewis Pair Moieties for Catalytic Hydrogenation of CO₂ in Functionalized UiO-66. *ACS Catalysis* **2015**, 5 (10), 6219-6229.
22. Zhao, X.; Wang, J.; Yang, M.; Lei, N.; Li, L.; Hou, B.; Miao, S.; Pan, X.; Wang, A.; Zhang, T., Selective Hydrogenolysis of Glycerol to 1,3-Propanediol: Manipulating the Frustrated Lewis Pairs by Introducing Gold to Pt/WO_x. **2017**, 10 (5), 819-824.
23. Lee, H.; Choi, Y. N.; Lim, D. W.; Rahman, M. M.; Kim, Y. I.; Cho, I. H.; Kang, H. W.; Seo, J. H.; Jeon, C.; Yoon, K. B., Formation of Frustrated Lewis Pairs in Ptx-Loaded Zeolite NaY. *Angewandte Chemie-International Edition* **2015**, 127 (44), 13272-13276.
24. Mahdi, T.; Stephan, D. W., Facile Protocol for Catalytic Frustrated Lewis Pair Hydrogenation and Reductive Deoxygenation of Ketones and Aldehydes. **2015**, 54 (29), 8511-8514.
25. Trunk, M.; Teichert, J. F.; Thomas, A., Room-Temperature Activation of Hydrogen by Semi-immobilized Frustrated Lewis Pairs in Microporous Polymer Networks. *Journal of the American Chemical Society* **2017**, 139 (10), 3615-3618.
26. Zhang, S.; Huang, Z.-Q.; Ma, Y.; Gao, W.; Li, J.; Cao, F.; Li, L.; Chang, C.-R.; Qu, Y., Solid frustrated-Lewis-pair catalysts constructed by regulations on surface defects of porous nanorods of CeO₂. *Nature Communications* **2017**, 8 (1), 15266.
27. Huang, Z.-Q.; Liu, L.-P.; Qi, S.; Zhang, S.; Qu, Y.; Chang, C.-R., Understanding All-Solid Frustrated-Lewis-Pair Sites on CeO₂ from Theoretical Perspectives. *ACS Catalysis* **2018**, 8 (1), 546-554.
28. Ghuman, K. K.; Hoch, L. B.; Szymanski, P.; Loh, J. Y. Y.; Kherani, N. P.; El-Sayed, M. A.; Ozin, G. A.; Singh, C. V., Photoexcited Surface Frustrated Lewis Pairs for Heterogeneous Photocatalytic CO₂ Reduction. *Journal of the American Chemical Society* **2016**, 138 (4), 1206-1214.
29. Ghossoub, M.; Yadav, S.; Ghuman, K. K.; Ozin, G. A.; Singh, C. V., Metadynamics-Biased ab Initio Molecular Dynamics Study of Heterogeneous CO₂ Reduction via Surface Frustrated Lewis Pairs. *ACS Catalysis* **2016**, 6 (10), 7109-7117.
30. Stephan, D. W.; Erker, G., Frustrated Lewis pair chemistry: development and perspectives. *Angewandte Chemie-International Edition* **2015**, 54 (22), 6400-6441.
31. Hunger, M., Multinuclear solid-state NMR studies of acidic and non-acidic hydroxyl protons in zeolites.

- Solid State Nuclear Magnetic Resonance* **1996**, *6* (1), 1-29.
32. Zheng, A.; Liu, S.-B.; Deng, F., P-31 NMR Chemical Shifts of Phosphorus Probes as Reliable and Practical Acidity Scales for Solid and Liquid Catalysts. *Chemical Reviews* **2017**, *117* (19), 12475-12531.
 33. Muller, M.; Harvey, G.; Prins, R., Quantitative multinuclear MAS NMR studies of zeolites. *Microporous and Mesoporous Materials* **2000**, *34* (3), 281-290.
 34. Buchholz, A.; Wang, W.; Xu, M.; Arnold, A.; Hunger, M., Thermal stability and dehydroxylation of Brønsted acid sites in silicoaluminophosphates H-SAPO-11, H-SAPO-81 H-SAPO-31, and H-SAPO-34 investigated by multi-nuclear solid-state NMR spectroscopy. *Microporous and Mesoporous Materials* **2002**, *56* (3), 267-278.
 35. Shen, W.; Li, X.; Wei, Y.; Tian, P.; Deng, F.; Han, X.; Bao, X., A study of the acidity of SAPO-34 by solid-state NMR spectroscopy. *Microporous and Mesoporous Materials* **2012**, *158*, 19-25.
 36. Martins, G.; Berlier, G.; Coluccia, S.; Pastore, H.; Superti, G.; Gatti, G.; Marchese, L., Revisiting the nature of the acidity in chabazite-related silicoaluminophosphates: combined FTIR and ²⁹Si MAS NMR study. *The Journal of Physical Chemistry C* **2007**, *111* (1), 330-339.
 37. Wiper, P. V.; Amelse, J.; Mafra, L., Multinuclear solid-state NMR characterization of the Brønsted/Lewis acid properties in the BP HAMS-1B (H-[B]-ZSM-5) borosilicate molecular sieve using adsorbed TMPO and TBPO probe molecules. *Journal of Catalysis* **2014**, *316*, 240-250.
 38. Schroeder, C.; Siozios, V.; Mück-Lichtenfeld, C.; Hunger, M.; Hansen, M. R.; Koller, H., Hydrogen Bond Formation of Brønsted Acid Sites in Zeolites. *Chemistry of Materials* **2020**, *32* (4), 1564-1574.
 39. Lo, B. T.; Ye, L.; Qu, J.; Sun, J.; Zheng, J.; Kong, D.; Murray, C. A.; Tang, C. C.; Tsang, S. C. E., Elucidation of Adsorbate Structures and Interactions on Brønsted Acid Sites in H-ZSM-5 by Synchrotron X-ray Powder Diffraction. *Angewandte Chemie-International Edition* **2016**, *128* (20), 6085-6088.
 40. Lo, B.; Ye, L.; Chang, G.; Purchase, K.; Day, S.; Tang, C.; Mei, D.; Tsang, S., Dynamic modification of pore opening of SAPO-34 by adsorbed surface methoxy species during induction of catalytic methanol-to-olefins reactions. *Applied Catalysis B: Environmental* **2018**, *237*, 245-250.
 41. Zhao, P.; Ye, L.; Sun, Z.; Lo, B. T.; Woodcock, H.; Huang, C.; Tang, C.; Kirkland, A. I.; Mei, D.; Edman Tsang, S. C., Entrapped single tungstate site in zeolite for cooperative catalysis of olefin metathesis with Brønsted acid site. *Journal of the American Chemical Society* **2018**, *140* (21), 6661-6667.
 42. Zhao, P.; Fang, H.; Mukhopadhyay, S.; Li, A.; Rudić, S.; McPherson, I. J.; Tang, C. C.; Fairen-Jimenez, D.; Tsang, S. E.; Redfern, S. A., Structural dynamics of a metal-organic framework induced by CO₂ migration in its non-uniform porous structure. *Nature Communications* **2019**, *10* (1), 1-8.
 43. Jeanvoine, Y.; Ángyán, J. G.; Kresse, G.; Hafner, J., Brønsted acid sites in HSAPO-34 and chabazite: an ab initio structural study. *The Journal of Physical Chemistry B* **1998**, *102* (29), 5573-5580.
 44. Li, G.; Huang, L.; Yi, X.; Peng, Y.-K.; Tsang, S. C. E.; Zheng, A., A nonpolar solvent effect by CH₃/interaction inside zeolites: characterization, mechanism and concept. *Chemical Communications* **2018**, *54* (95), 13435-13438.
 45. Liu, L.; Lukose, B.; Jaque, P.; Ensing, B., Reaction mechanism of hydrogen activation by frustrated Lewis pairs. *Green Energy & Environment* **2019**, *4* (1), 20-28.
 46. Spies, P.; Erker, G.; Kehr, G.; Bergander, K.; Fröhlich, R.; Grimme, S.; Stephan, D. W., Rapid intramolecular heterolytic dihydrogen activation by a four-membered heterocyclic phosphane-borane adduct. *Chemical Communications* **2007**, (47), 5072-5074.
 47. Stephan, D. W., Frustrated Lewis pairs: from concept to catalysis. *Accounts of Chemical Research* **2015**, *48* (2), 306-316.
 48. Wang, W.; Hunger, M., Reactivity of surface alkoxy species on acidic zeolite catalysts. *Accounts of Chemical Research* **2008**, *41* (8), 895-904.
 49. Wang, C.; Chu, Y.; Xu, J.; Wang, Q.; Qi, G.; Gao, P.; Zhou, X.; Deng, F., Extra-Framework Aluminum-Assisted Initial C-C Bond Formation in Methanol-to-Olefins Conversion on Zeolite H-ZSM-5. *Angewandte Chemie-International Edition* **2018**, *130* (32), 10354-10358.
 50. Zhu, Q.; Kondo, J. N.; Ohnuma, R.; Kubota, Y.; Yamaguchi, M.; Tatsumi, T., The study of methanol-to-olefin over proton type aluminosilicate CHA zeolites. *Microporous and Mesoporous Materials* **2008**, *112* (1-3), 153-161.
 51. Goguen, P. W.; Xu, T.; Barich, D. H.; Skloss, T. W.; Song, W. G.; Wang, Z. K.; Nicholas, J. B.; Haw, J. F., Pulse-quench catalytic reactor studies reveal a carbon-pool mechanism in methanol-to-gasoline chemistry on zeolite HZSM-5. *Journal of the American Chemical Society* **1998**, *120* (11), 2650-2651.
 52. Zhao, X. B.; Wang, L. Y.; Li, J. Z.; Xu, S. T.; Zhang, W. N.; Wei, Y. X.; Guo, X. W.; Tian, P.; Liu, Z. M., Investigation of methanol conversion over high-Si beta zeolites and the reaction mechanism of their

- high propene selectivity. *Catalysis Science & Technology* **2017**, 7 (4), 5882-5892.
53. Shah, R.; Payne, M.; Lee, M.-H.; Gale, J. D., Understanding the catalytic behavior of zeolites: A first-principles study of the adsorption of methanol. *Science* **1996**, 271 (5254), 1395-1397.
 54. Jiang, Y. J.; Hunger, M.; Wang, W., On the reactivity of surface methoxy species in acidic zeolites. *Journal of the American Chemical Society* **2006**, 128 (35), 11679-11692.
 55. T. Xu; A. A. Kheir; Brookshier, M. A., Is HSAPO-34 a truly Bronsted acid site? In *16th International Congress on Catalysis*, Beijing, 2016.
 56. Qian, Q.; Vogt, C.; Mokhtar, M.; Asiri, A. M.; Al-Thabaiti, S. A.; Basahel, S. N.; Ruiz-Martínez, J.; Weckhuysen, B. M., Combined Operando UV/Vis/IR Spectroscopy Reveals the Role of Methoxy and Aromatic Species during the Methanol-to-Olefins Reaction over H-SAPO-34. *Chemcatchem* **2014**, 6 (12), 3396-3408.
 57. Matam, S. K.; Howe, R. F.; Thetford, A.; Catlow, C. R. A., Room temperature methoxylation in zeolite H-ZSM-5: an operando DRIFTS/mass spectrometric study. *Chemical Communications* **2018**, 54 (91), 12875-12878.
 58. Matam, S. K.; Nastase, S. A.; Logsdail, A. J.; Catlow, C. R. A., Methanol loading dependent methoxylation in zeolite H-ZSM-5. *Chemical Science* **2020**, 11 (26), 6805-6814.
 59. Farneth, W. E.; Gorte, R. J., Methods for Characterizing Zeolite Acidity. *Chemical Reviews* **1995**, 95 (3), 615-635.
 60. Ravi, M.; Sushkevich, V. L.; van Bokhoven, J. A., Towards a better understanding of Lewis acidic aluminium in zeolites. *Nature materials* **2020**, 19 (10), 1047-1056.
 61. Kramer, G. J.; van Santen, R. A.; Emeis, C. A.; Nowak, A. K., Understanding the acid behaviour of zeolites from theory and experiment. *Nature* **1993**, 363 (6429), 529-531.
 62. Gounder, R.; Iglesia, E., Catalytic Consequences of Spatial Constraints and Acid Site Location for Monomolecular Alkane Activation on Zeolites. *Journal of the American Chemical Society* **2009**, 131 (5), 1958-1971.
 63. Sun, Q.; Wang, N.; Bing, Q.; Si, R.; Liu, J.; Bai, R.; Zhang, P.; Jia, M.; Yu, J., Subnanometric Hybrid Pd-M(OH)₂, M = Ni, Co, Clusters in Zeolites as Highly Efficient Nanocatalysts for Hydrogen Generation. *Chem* **2017**, 3 (3), 477-493.
 64. Chai, Y.; Shang, W.; Li, W.; Wu, G.; Dai, W.; Guan, N.; Li, L., Noble Metal Particles Confined in Zeolites: Synthesis, Characterization, and Applications. *Advanced Science* **2019**, 6 (16), 1900299.
 65. Silaghi, M.-C.; Chizallet, C.; Raybaud, P., Challenges on molecular aspects of dealumination and desilication of zeolites. *Microporous and Mesoporous Materials* **2014**, 191, 82-96.
 66. Xu, J.; Wang, Q.; Deng, F., Metal Active Sites and Their Catalytic Functions in Zeolites: Insights from Solid-State NMR Spectroscopy. *Accounts of Chemical Research* **2019**, 52 (8), 2179-2189.
 67. Yi, X.; Liu, K.; Chen, W.; Li, J.; Xu, S.; Li, C.; Xiao, Y.; Liu, H.; Guo, X.; Liu, S.-B.; Zheng, A., Origin and Structural Characteristics of Tri-coordinated Extra-framework Aluminum Species in Dealuminated Zeolites. *Journal of the American Chemical Society* **2018**, 140 (34), 10764-10774.
 68. Vjunov, A.; Fulton, J. L.; Huthwelker, T.; Pin, S.; Mei, D.; Schenter, G. K.; Govind, N.; Camaioni, D. M.; Hu, J. Z.; Lercher, J. A., Quantitatively Probing the Al Distribution in Zeolites. *Journal of the American Chemical Society* **2014**, 136 (23), 8296-8306.
 69. Ortalan, V.; Uzun, A.; Gates, B. C.; Browning, N. D., Direct imaging of single metal atoms and clusters in the pores of dealuminated HY zeolite. *Nature Nanotechnology* **2010**, 5 (7), 506-510.
 70. Ye, L.; Teixeira, I.; Lo, B. T.; Zhao, P.; Tsang, S. E., Spatial differentiation of Brønsted acid sites by probe molecule in zeolite USY using synchrotron X-ray powder diffraction. *Chemical Communications* **2017**, 53 (70), 9725-9728.
 71. Dědeček, J.; Čapek, L.; Kaucký, D.; Sobalík, Z.; Wichterlová, B., Siting and Distribution of the Co Ions in Beta Zeolite: A UV-Vis-NIR and FTIR Study. *Journal of Catalysis* **2002**, 211 (1), 198-207.
 72. Mota, C. J.; Bhering, D. L.; Rosenbach, N., Jr., A DFT study of the acidity of ultrastable Y zeolite: where is the Bronsted/Lewis acid synergism? *Angewandte Chemie-International Edition* **2004**, 43 (23), 3050-3.
 73. Collignon, F.; Jacobs, P. A.; Grobet, P.; Poncelet, G., Investigation of the Coordination State of Aluminum in β Zeolites by X-ray Photoelectron Spectroscopy. *The Journal of Physical Chemistry B* **2001**, 105 (29), 6812-6816.
 74. van Bokhoven, J. A.; van der Eerden, A. M. J.; Koningsberger, D. C., Three-Coordinate Aluminum in Zeolites Observed with In situ X-ray Absorption Near-Edge Spectroscopy at the Al K-Edge: Flexibility of Aluminum Coordinations in Zeolites. *Journal of the American Chemical Society* **2003**, 125 (24), 7435-7442.

75. Brus, J.; Kobera, L.; Schoefberger, W.; Urbanova, M.; Klein, P.; Sazama, P.; Tabor, E.; Sklenak, S.; Fishchuk, A. V.; Dedecek, J., Structure of Framework Aluminum Lewis Sites and Perturbed Aluminum Atoms in Zeolites as Determined by Al-27{H-1} REDOR (3Q) MAS NMR Spectroscopy and DFT/Molecular Mechanics. *Angewandte Chemie-International Edition* **2015**, 54 (2), 541-545.
76. Amakawa, K.; Wrabetz, S.; Kröhnert, J.; Tzolova-Müller, G.; Schlögl, R.; Trunschke, A., In Situ Generation of Active Sites in Olefin Metathesis. *Journal of the American Chemical Society* **2012**, 134 (28), 11462-11473.
77. Pantazidis, A.; Burrows, A.; Kiely, C. J.; Mirodatos, C., Direct evidence of active surface reconstruction during oxidative dehydrogenation of propane over VMgO catalyst. *Journal of Catalysis* **1998**, 177 (2), 325-334.